Current Research in Food Science 7 (2023) 100587

Contents lists available at ScienceDirect

Current Research in Food Science

journal homepage: www.sciencedirect.com/journal/current-research-in-food-science

Identifying the quality characteristics of pork floss structure based on deep learning framework

Che Shen [a,b,1], Meiqi Ding [a,1], Xinnan Wu [a], Guanhua Cai [a], Yun Cai [a], Shengmei Gai [a], Bo Wang [a,c,d,*], Dengyong Liu [a,**]

[a] College of Food Science and Technology, Bohai University, Jinzhou 121013, China
[b] Key Laboratory for Agricultural Products Processing of Anhui Province, School of Food Science and Engineering, Hefei University of Technology, Hefei, 230009, China
[c] Key Laboratory of Meat Processing and Quality Control, MOE, Key Laboratory of Meat Processing, MARA, College of Food Science and Technology, Nanjing Agricultural University, Nanjing 210095, China
[d] Institute of Ocean Research, Bohai University, Jinzhou 121013, Liaoning, China

ARTICLE INFO

Keywords:
Deep learning
Pork floss
Machine vision
Sensory evaluation
Image segmentation

ABSTRACT

Pork floss is a traditional Chinese food with a long history. Nowadays, pork floss is known to consumers as a leisure food. It is made from pork through a unique process in which the muscle fibers become flaky or granular and tangled. In this study, a deep learning-based approach is proposed to detect the quality characteristics of pork floss structure. Describe that the experiments were conducted using widely recognized brands of pork floss available in the grocery market, omitting the use of abbreviations. A total of 8000 images of eight commercially available pork flosses were collected and processed using sharpening, image gray coloring, real-time shading correction, and binarization. After the machine learning model learned the features of the pork floss, the images were labeled using a manual mask. The coupling of residual enhancement mask and region-based convolutional neural network (CRE-MRCNN) based deep learning framework was used to segment the images. The results showed that CRE-MRCNN could be used to identify the knot features and pore features of different brands of pork floss to evaluate their quality. The combined results of the models based on the sensory tests and machine vision showed that the pork floss from TC was the best, followed by YJJ, DD and HQ. This also shows the potential of machine vision to help people recognize the quality characteristics of pork floss structure.

1. Introduction

Pork floss (Zhu Rou Song) has been a traditional food in China for hundreds of years (Wang et al., 2023). At present, it is well-known to Chinese consumers because it is a leisure food that can be found everywhere. It is a kind of meat product made of fresh lean meat, which is formed into flakes or muscle fiber bundles through several processes such as pretreatment, cooking, beating, seasoning and frying. The requirements for high-quality pork floss are flocculent, soft, and fluffy fibers, with a few knots allowed (Chinese Standards, 2009). The "fluffiness" of meat floss is mainly reflected in the porous medium (porous structure) formed by the random arrangement of protein fibers, which is mainly composed of protein fibers and air (Li et al., 2021). This fluffy and porous structure is also a unique structural feature of pork floss (Li et al., 2021). The pore structure is the characteristic feature of porous media, but also the form of the existence of porous media. In general, the pores of porous media are arranged in an irregular two-dimensional network (Esser et al., 2021). The knots are the unloosened part of the muscle fiber. High temperatures and tossing cause varying degrees of loosening of muscle bundles and myogenic fibers of pork during roasting. However, uneven panning or high temperatures cause the myogenic fibers to form unopened tangles. The presence of knots affects the fluffiness of pork floss. Pore size, pore number, and pore distribution are general characteristics obtained from

* Corresponding author. College of Food Science and Technology, Bohai University, No. 19, Keji Rd., New Songshan District, Jinzhou 121013, Liaoning Province, China.
** Corresponding author. College of Food Science and Technology, Bohai University, No. 19, Keji Rd., New Songshan District, Jinzhou 121013, Liaoning Province, China.
E-mail addresses: daqingwb@163.com (B. Wang), jz_dyliu@126.com (D. Liu).
[1] Che Shen and Meiqi Ding contributed equally to this work and should be considered co-first authors.

https://doi.org/10.1016/j.crfs.2023.100587
Received 6 July 2023; Received in revised form 4 September 2023; Accepted 5 September 2023
Available online 9 September 2023

the pore structure of porous media (Münch and Holzer, 2010; Fu et al., 2021). The total knots area, the total circumference of knots, and the number of knots were extracted from the knot features based on the degree of looseness of muscle fibers. The pore and knot characteristics are closely related to the mechanical properties, which are important for sensory quality of pork floss, characterization of pork floss and quality evaluation.

In recent years, machine vision-based image processing methods have been widely used for visual food quality assessment (Li et al., 2018; Taheri-Garavand, Fatahi, Shahbazi and de la Guardia, 2019). In contrast to traditional food structure evaluation by sensory assessors, machine vision can determine information about color, texture, shape, and other food structure characteristics more quickly and accurately, and can quantitatively analyze this feature information (Taheri-Garavand et al., 2019a,b).

The Convolutional Neural Network (CNN) is a deep learning method with hierarchical feature learning capability that has made a significant breakthrough in image analysis (Ali et al., 2014; Lecun et al., 2015). Meanwhile, image segmentation methods based on neural network techniques are receiving increasing attention and improved algorithms, such as Fast R–CNN (Girshick, 2015), Mask R–CNN (He et al., 2017), which achieve better and faster results than typical CNNs in object recognition. Based on Mask R–CNN, a new image segmentation algorithm, Coupling Residual Enhancement-Mask Region CNN (CRE-MRCNN), is proposed in this study.

Therefore, the first objective of this study was that CRE-MRCNN was applied to images of commercial pork floss. Image segmentation was used to extract knot features and pore features from commercial pork floss to evaluate quality. The second objective was to develop a machine vision-oriented evaluation model with a higher weighting of machine vision judgment and a sensory test-oriented evaluation model with a higher weighting of sensory characteristics judgment to evaluate and rank selected commercially available pork floss based on a gradient descent algorithm.

2. Materials and methods

2.1. Experimental samples

The eight most common and widely sold brands of pork floss in the grocery market were investigated, labeled as DD, HQ, LYW, MZX, SS, TC, WSM, and YJJ. They were purchased from the Jingdong online shopping mall (Jingdong.com), Taobao online shopping mall (Taobao.com), and RT-Mart supermarket in Jinzhou, Liaoning. The total amount of each brand was 5.5 kg.

2.2. Deep learning-based framework for pork floss structure recognition

The specifics and process of the deep learning framework for identifying the structural features of pork flosses are described. Fig. 1 illustrates the overall process of the proposed deep learning-based framework, including the following steps: data acquisition, data preprocessing, deep learning architecture creation, and result analysis. The dataset is obtained from the image acquisition and image preprocessing steps. Subsequently, the CRE-MRCNN model was used to identify the structure of eight brands of pork flosses from the dataset and compared with several other models. Finally, the image segmentation structures were evaluated as well as extracting features of the pork flosses, including knot features and pore features of the pork flosses. Detailed information is described in the following sections.

2.2.1. Image acquisition

So that the pork floss is evenly distributed in the cylindrical shape, the three-dimensional structure of the pork floss is fully restored, and the porous structure of the pork floss is better expressed. As shown in Fig. 2, 10 g of pork floss of each brand was weighed and uniformly shaken into a cylindrical mold with a diameter of 10 cm and a height of 5 cm until the mold was filled. The mold was placed on the sample support plate, which was directly below the center of the ring-shaped shadowless lamp and lens. To obtain the maximum pore structure of the pork floss, the light intensity of the shadowless ring lamp must be adjusted. The digital image signal of the pork floss was captured by the CDD industrial camera, transferred to the computer via the Ethernet port, and the captured images were stored and analyzed in PNG format using the image processing system KV-X (Suzhou Kelvis Automation Technology Co., Ltd., Suzhou, Jiangsu). The pixel size of the RGB images captured by the CCD camera was 2448 pixels (W) × 2048 pixels (H) with a bit depth of 24.

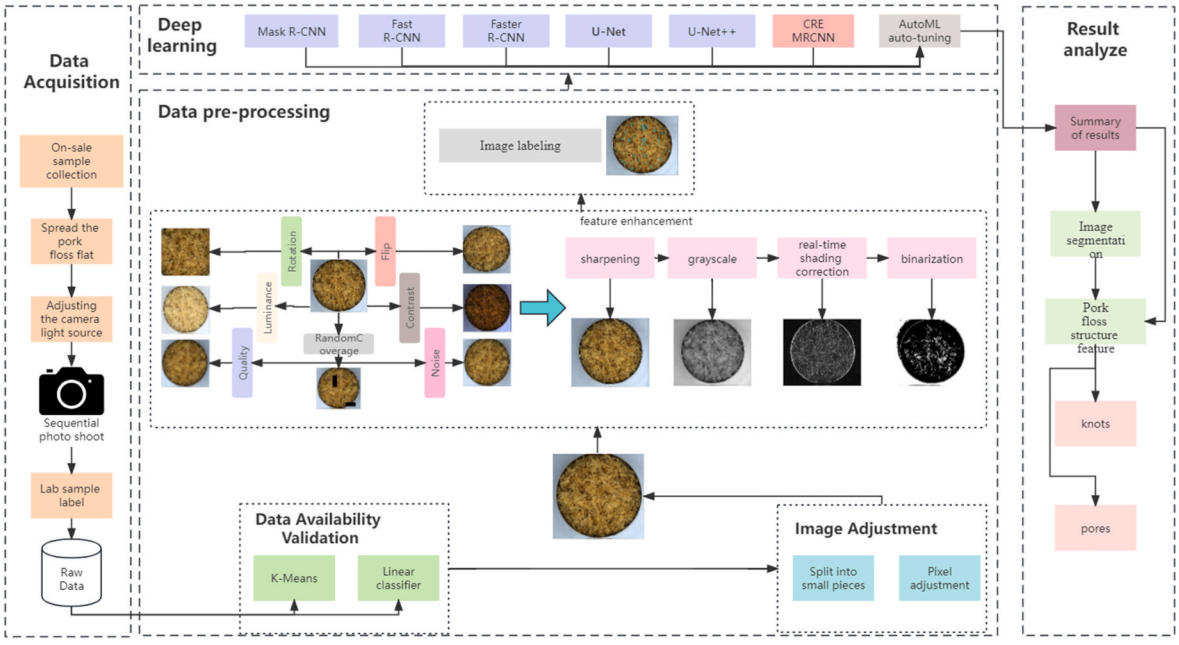

Fig. 1. Overview of the deep learning-based framework.

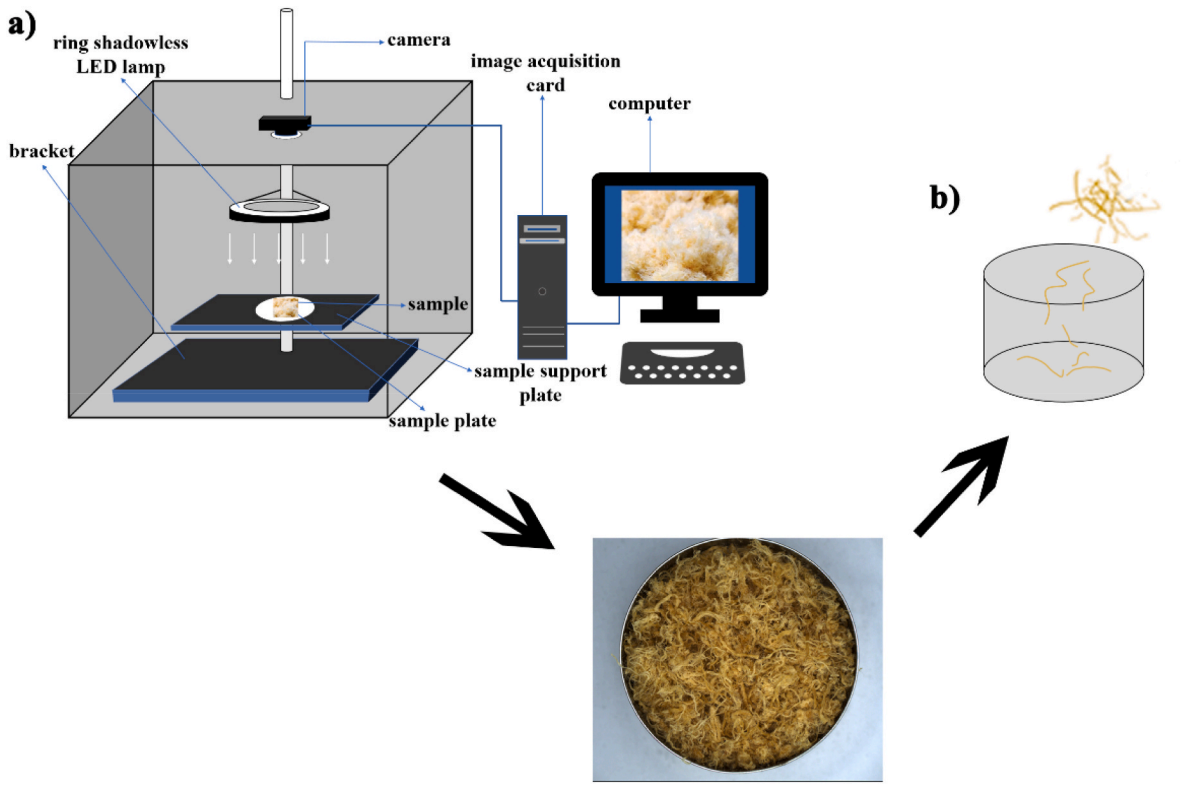

Fig. 2. Construction of computer vision system.

2.2.2. Image pre-processing

The core technology of machine vision mainly refers to image processing and analysis. Image processing consists of a series of image operations that improve image quality to eliminate image errors caused by, for example, geometric distortion, improper focusing, repetitive noise, uneven illumination, and camera motion. Image analysis is the

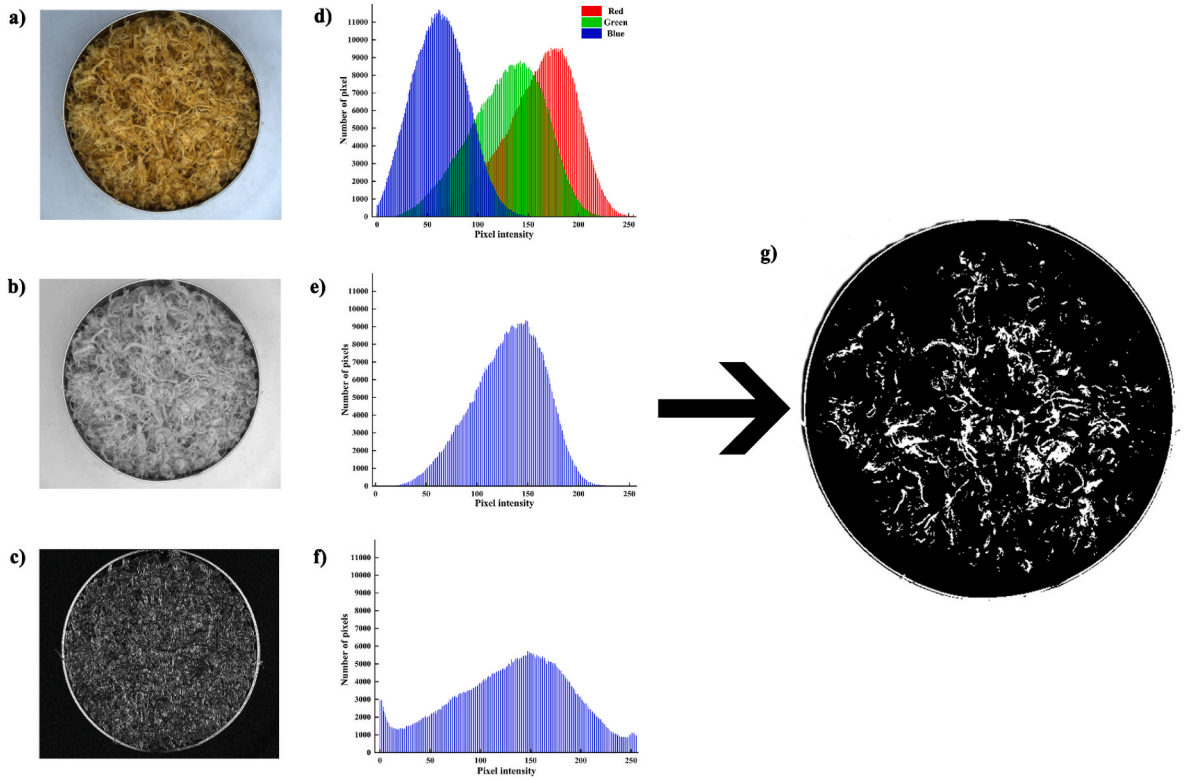

Fig. 3. Pork floss image pre-processing. (a) Sharpened image; (b) grayscale image; (c) image of real-time shading correction; (d) histogram of the sharpened image; (e) histogram of the grayscale image; (f) histogram of the real-time shading correction image; (g) binarization-processed image.

process of identifying the target (That is, the ROI portion of the selected) against the background and generating quantitative information that is used for subsequent control system decisions (Zhang et al., 2020). Due to the low and indistinguishable gray scale contrast between some knots and the non-knots part of the pork floss in the original images, it was necessary to sharpen all images of pork floss captured by the CCD industrial camera.

The ROI regions of the sharpened images were intercepted with five random image regions of 900 pixels × 900 pixels on the left, right, top, bottom and center of the images. 500 original images of each mark were collected. After intercepting ROI, 1000 images were collected for each brand, so that a total of 8000 images were collected for eight brands of pork floss. As a representation of color features in images, histograms are commonly used to express the information distribution of pixel intensities in digital images (Javadi et al., 2020). In an image, each pixel contains three groups of information, namely the R value, the G value, and the B value. The RGB values of the sharpened pork floss image (Fig. 3a) were extracted using machine vision, and the information obtained about the intensity of the pixels was plotted using a histogram (Fig. 3d). The pixel values of the image range from 0 to 255, the horizontal axis represents the change in dimension or hue and the vertical axis represents the total number of pixels in the image.

Converting multi-channel RGB color images containing luminance and color to a single-channel grayscale image is important to improve contrast between target and background information, increase efficiency, and make the computation. The grayscale image obtained by processing grayscale images is also called a monochrome image. The effect of converting a multi-channel RGB color image into a single-channel gray image is shown in Fig. 3b. After detection by machine vision, the histogram of the grayscale image has only one color because the R value of the processed grayscale image is equal to the G and B values, i.e., R = G = B (Fig. 3e). The histogram of the grayed-out image is mainly concentrated in the range of 30–200. Since pork floss is filamentous, the images captured by the industrial camera are affected by non-uniform illumination and non-uniform reflections on the product surface. The images of pork floss are also difficult to be processed by the image processing software due to the uneven illumination, which results in the contrast of the local or global information in the processed gray scale images not being clear enough.

Differentiation of the imputed background image is performed using real-time shading correction to eliminate shadows in the variable background and retain only those areas with abrupt contrast changes. The specific operations were: Reducing the original image and then filtering the reduced image; Restoring the filtered image to its original size; and differentiating the original image and the filtered reduced image. The real-time shading correction algorithm was applied to remove the background shadows while preserving the defects. This solved the problems of uneven illumination and inconsistent reflections on the product surface during photo capture caused by the filamentous structure of pork floss. Real-time shading correction can remove background shadows by preserving areas with abrupt contrast changes, as shown in Fig. 3c. The gray levels of the histogram of the image with pork floss after shading correction achieve an “approximately” balanced distribution in the range of 0–255 (Fig. 3f). This achieved the purpose of increasing the contrast between the foreground and background and highlighting the texture of the pork floss. This is because the process of real-time shading correction increases the overall contrast of the image and makes it possible to preserve the local details of the image.

The basic principle of converting a grayscale image into a binarized image is to take only two values of the grayscale values of the image pixel points to achieve the effect of a black and white image. Inter-mode as a global binarization method is based on the assumption that the histogram is a bimodal pattern histogram. The histogram is smoothed and filtered several times until only the two largest peaks J and K remain, then the threshold value is $T = (J + K)/2$. According to the practical needs, the system uses the inter-modes method of the global binarization method to binarize the shadow corrected image and separate the pores from the background. White is used as the background and black is the pore area. The clarity of the image with the distribution of pork floss features depends on the effect of image binarization. Therefore, the image subjected to real-time shading correction should be subsequently processed using binarization to obtain the feature distribution of pork floss. As shown in Fig. 3g, the binarized image extracted the pork floss region from the background area, eliminated shadows and background noise, better preserved the pork floss structure, and identified the pork floss pores.

2.2.3. Image labeling

The knots of pork floss are an important component of quality characteristics assessment. Since the pork floss image dataset in this work does not have corresponding segmentation labels for the knots, the images without labels cannot be trained for the network. Therefore, a small segmentation dataset must be created for training by first manually masking the images for labeling. Knots are the unloosened part of muscle fibers that tend to form clumps, resulting in the computer vision systems not being able to easily identify the parts with and without knots. This requires a manually defined description of the knots. Knots should be defined as the unloosened, clumped portion of muscle fibers and tendon fragments. Knots of pork floss are irregular objects that were finely labeled using polygon frames to generate a JSON file containing the image labeling information, including the position coordinates of the target knot (the position of the pixel of the target object), the category label of the target object, and the image size information. The labeled pork floss of each mark contained 400 images each with a pixel size of 900 × 900. The whole image set was divided into training and testing sets: 80% for training and 20% for testing. The training set consisted of 2560 randomly selected images and the test set consisted of 640 randomly selected images.

2.2.4. CRE-MRCNN framework construction

Mask Region-based Convolutional Neural Network (Mask R–CNN) is a Deep Learning-based model for target recognition and semantic segmentation, which is an extended version of the Faster Region-based Convolution Neural Networks (Faster R–CNN) model proposed by Ren et al. (2017). Compared to Faster R–CNN, Mask R–CNN not only detects objects in an image, but also generates a binary segmentation map for each object, which is used to represent the exact position of the object. The Mask R–CNN model consists of three main components: a feature extraction network, a region proposal network (RPN), and a target detection branch. The feature extraction network typically uses a pre-trained convolutional neural network such as ResNet to extract features from the image, and the RPN is used to generate candidate regions and perform classification and regression on these candidate regions to determine the final recognition results. The target recognition branch then classifies and regresses each candidate region and generates a binary segmentation map for each region. The model produces a segmentation of the target pork floss image that matches the size and shape of the target node. The final detection and results are combined to obtain 1 segmented image that contains the target node class and matches the size and shape of the target node.

Meanwhile, in this study, a new semantic segmentation algorithm, Coupling Residual Enhancement-Mask Region CNN (CRE-MRCNN) is proposed. To address the unique challenges posed by burnt regions and knot regions in pork floss images, this model combines multiple strategies, including contextual matching, data augmentation, and specialized region analysis, with the aim of better adapting to the distinctive characteristics of pork floss images. We simulated real industrial production conditions to obtain more representative training data. By incorporating data augmentation techniques, we successfully enhanced image quality, enabling the model to handle color, texture, and other variability factors more effectively. In terms of details, as shown in Fig. 4, the CRE-MRCNN model consists of four major components: encoding, binarization

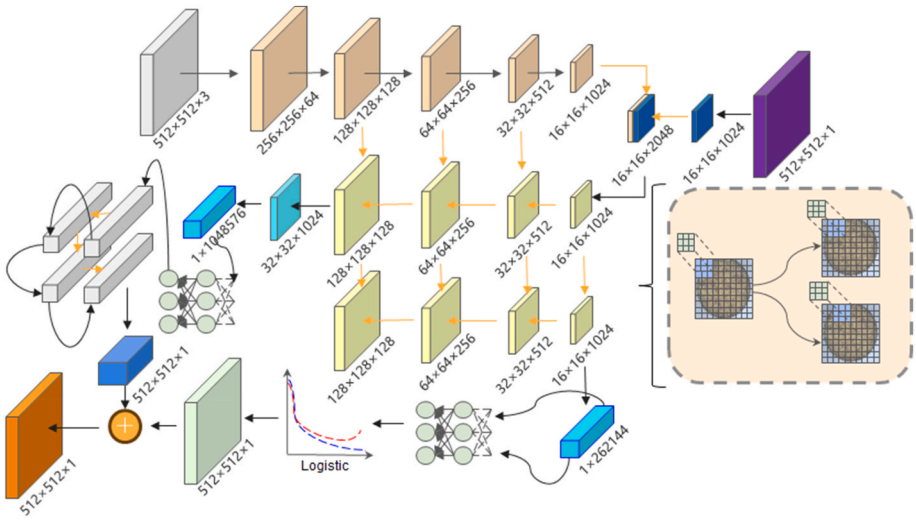

Fig. 4. CRE-MRCNN model framework.

intervention, decoding, and feature fusion.

1). The Encoding component comprises five convolutional layers, starting from input data of size 512 × 512 × 3. Each layer involves a 3 × 3 convolutional kernel, with several convolutional filters equal to 64 multiplied by the current layer index, followed by 2 × 2 Max Pooling. This process continues until the Encoding component outputs a feature map of size 16 × 16 × 1024.
2). The Binarization Intervention process includes a convolutional layer and a concatenation layer. The convolutional layer processes the binarized image using an 8 × 8 convolutional kernel, stride of 8, and 1024 convolutional filters. After a subsequent 4 × 4 Max Pooling, the resulting feature map matches the size of the output from the Encoding component. It is then concatenated along the channel axis to yield a 16 × 16 × 2048 feature map.
3). The Decoding component consists of two sets of four-layer convolutional neural networks, with the same number of convolutional filters as in the encoder. However, these networks utilize dilated convolutions with a dilation rate of 2.
4). The Feature Fusion part involves two pathways. One pathway converts the 16 × 16 × 1024 feature map into a one-dimensional feature vector, which is then passed through a fully connected neural network with the same number of neurons, followed by logistic regression. The reshaped result forms a 512 × 512 × 1 mask feature map. The second pathway stretches the 32 × 32 × 1024 feature map into a one-dimensional feature vector, which then undergoes residual computation through four 1D CNNs before being processed by an Attention mechanism. This pathway also results in a reshaped 512 × 512 × 1 mask feature map. Ultimately, the two feature maps are element-wise summed to obtain the final segmentation result.

CRE-MRCNN combines the strengths of Mask R–CNN and Faster R–CNN, autonomously identifying regions of interest and generating pixel-level precise segmentation results. This has enabled us to achieve higher accuracy and reliability in the detection and segmentation tasks for fibers structure of pork floss.

A comparative study was conducted to examine the performance of CRE-MRCNN compared to other methods in pork floss of structure identification and extracted feature. As Faster R–CNN (Ren et al., 2017), U-Net++ (Zhou et al., 2018), UNet 3+ (Huang et al., 2020), Mask R–CNN (He et al., 2017), and Cascade Mask R–CNN (Cai and Vasconcelos, 2021), are commonly chosen in the study of segmenting images, they are selected for this experiment.

2.2.5. Implementation details

In this study, we used image patch size of 512 × 512 × 3 and binarized image size of 512 × 512 × 1. Following AutoML-based hyperparameter tuning, the optimal configuration is as follows: batch size of 32, Mask confidence threshold of 0.74, learning rate of 1e-4, activation function of LeakyReLU with a leakage coefficient of 0.2, the loss function of Dice with equal weights for all losses, the optimization function of Adam with β coefficients (0.479, 0.999). All models were trained for 200 epochs and tested on Ubuntu 20.04, using a NVIDIA Tesla V100.

2.2.6. Image segmentation evaluation

To quantitatively analyze the effect of intersection segmentation, the commonly used metric for evaluating image segmentation, Intersection over Union (IoU), is used to evaluate intersection. IoU is a metric that visualizes the area of overlap between predicted image A and calibration image B. It is used to evaluate the overlap between two rectangular images (Song et al., 2021). The output of each image and its true edge IoU are given by using CRE-MRCNN for the segmentation of 640 samples of each brand pork floss for knot segmentation, and further the obtained IoU values of each image are re-averaged as the overall segmentation accuracy of the model, the IoU coefficients are calculated as shown in equation (1):

$$IoU = \frac{S_{pred} * S_{gt}}{(S_{pred} + S_{gt}) - S_{pred} * S_{gt}} \quad (1)$$

where S_{pred} is the region of the segmentation result and S_{gt} is the manually labeled region.

The IoU coefficient is used to quantify the degree of identity between finite sample sets. The higher the coefficient, the more similar the segmentation result and the corresponding marked true result are.

2.2.7. Pork floss feature extraction

Knot and pore characteristics are a relatively common method for evaluating the microstructure of pork floss. The pork floss image was segmented using the CRE-MRCNN model to produce a series of branches, all of which were binary images of the pork floss knots detected in the original image. Thus, if there is an H × W × 3 image of knots in which n knots are detected, the CRE-MRCNN segmentation generates a branch that produces an H × W × n image. Each pixel point in this image takes the value 0 or 1. If the value is 1, it means that the point is in the region of pork floss knots; otherwise, it means that the point is a pixel point that forms the background. To realize the conversion between pixels and standard-length units, 19.4 pixels = 1 mm

was calculated. The perimeter, area, average area and number were calculated for the segmented image of the segmented knots.

The pore features of pork floss, including porosity, number of pores, average pore area, and pore size distribution, were extracted using the CRE-MRCNN model for binarized image segmentation. The size of the feature values was calculated in mm^2, and 19.4 pixels = 1 mm. The coefficient of variation is a measure of the degree of representativeness of the mean and a measure of the dispersion of the distribution of response variables and the balance of the evolution of things. The homogeneity of the pore distribution on the same image was evaluated by performing a coefficient of variation analysis for five randomly intercepted pore data with the same area size on the same image (Shenoy et al., 2015). Repeatability of pore data was also evaluated by performing an analysis of the coefficient of variation for pore data from ten image sets of the same brand of pork floss.

2.3. Sensory testing

Sensory analyzes were performed according to the procedures described by Shen et al. (2023) and Cai et al. (2021). A total of 30 sensory assessors underwent an initial screening process (including matching and ranking tests) and nine training sessions on descriptors and methods specific to pork floss, followed by selection of a final group of 19 consumers who consume pork floss at least once per week as assessors (9 men and 10 women). After discussion with the group members, the following descriptors of the quality characteristics of the pork floss were established: (1) knot size is defined as the size of the unloose part of the muscle fiber and tendon fragments of the pork floss; (2) fluffiness: the degree to which the finished pork floss is soft and fluffy like cotton in its natural state; (3) thickness: the thickness of the muscle fiber in the finished pork floss; (4) uniformity: the uniform distribution of tissues of the finished pork floss; (5) coarseness: the unevenness of the muscle fiber surface of the pork floss; (6) hardness: the degree of hardness of the muscle fiber of the finished pork floss; (7) color consistency: the finished pork floss is golden yellow, and there is no color difference in the distribution of the pork floss that can be seen by the naked eye; (8) intactness: the pork floss is fluffy, complete into a lump, and has no powder; (9) liking: the comprehensive liking of pork floss. The strength of each attribute was rated on a linear (unstructured) scale of 10 cm, with "none" on the left and "strong" on the right. Samples of pork floss of each brand were provided to the trained panelists in five sessions, and the sessions consisted of eight rounds of observations. 10 g of pork floss from different brands were shaken in 200 mL sensory cups, and each sensory cup was randomly labeled with three numbers. Five sensory evaluations were conducted for each brand of pork floss, three replicates of pork floss in each brand were provided for each session, and the results were statistically analyzed.

2.4. Comprehensive evaluation model

Weight is a numerical value used to measure the extent of the role of each marker value in the total and is indicative of the importance of an indicator item in the indicator item system. Similarly, it indicates how a change in that indicator term affects the results when the associated baseline indicator term does not change. It is necessary to establish a comprehensive quality characteristics evaluation system based on the pore and knot index system of pork floss and the sensory evaluation of pork floss, respectively, to provide an objective, accurate and scientific evaluation of the fluffy performance presented by pork floss.

In this study, gradient descent was used to calculate the weights for each column of data. The optimal weights were determined by first defining the loss function and then minimizing the loss function by continuously adjusting the weights. In this problem, mean square error (MSE) was used as the loss function, as shown in Eq. (2):

$$loss = \frac{1}{2} m * \boldsymbol{sum}((\mathbf{w_1} * x_1 + w_2 * x_2 + \ldots + w_n * x_n - S) * 2) \quad (2)$$

where m is the number of samples, w_1, w_2, …, w_n are the weights of each column of data, x_1, x_2, …, x_n are the values of each column of data, and S is the score value of each data. The optimal weights are obtained by continuously adjusting the weights to minimize the loss function.

The core idea of gradient descent is to adjust the weights by continuous iteration in the direction of the decreasing loss function. This is done in the following steps: i. Initialize the weights w_1, w_2, …, w_n with a standard normal distribution; ii. Calculate the gradient (i.e., partial derivative) of the loss function loss for each weight w_i, as shown in Eq. (3):

$$\frac{dLoss}{dw_i} = \frac{1}{m} * \boldsymbol{sum}((\boldsymbol{w_1} * x_1 + w_2 * x_2 + \ldots + w_n * x_n - S) * x_i) \quad (3)$$

iii adjust the value of each weight according to the gradient descent update rule, as shown in Eq. (4):

$$w_i = w_i - learning\_rate * \frac{dloss}{dw_i} \quad (4)$$

where the learning rate is the increment of the update at each iteration in this paper it is 0.001.

Repeat steps ii and iii up to 1000 rounds of training. Finally, the weights of each attribute are generated.

2.5. Statistical analysis

All statistical data were analyzed by IBM SPSS Statistics 26 software (SPSS Inc., Chicago, IL, USA). 500 original images of pork floss from each brand were captured, and after capturing ROI, each brand had pork floss 1000 images. Differences among samples were compared by using least significant difference (LSD) test ($P < 0.05$) and Tukey's HSD test (Honestly significant difference) ($P < 0.05$). Results are reported as mean the means ± standard error (S.E.).

3. Results

3.1. Segmentation results

Pores and knots are important features of pork floss structure and influence the quality evaluation of pork floss structure. However, when processing pork floss image pairs, the pores are easy to identify, and evaluation of pork floss pore segmentation results is not required. Only the labeled knots need to be evaluated. As shown in Fig. 5a, the nodal heads of the pork floss were in the manually labeled image. The model CRE-MRCNN learned the features of the knot and non-knots in pork floss to segment the pork floss image. As shown in Fig. 5b, the white part is the pore part, while the red part is the knot feature, and the black part is the non-knot part in the pork floss. As you can see, the model CRE-MRCNN can identify the knots of pork floss and thus evaluate the quality characteristics of each brand of pork floss.

The IoU results for the output borders and the real edges of all test images are shown in Fig. 5c. It can be seen that the IoU value of contour segmentation in the knots after image segmentation shows a fluctuating trend, with the minimum at 84.23% and the maximum at 97.23%. However, the average accuracy of the whole model was 92.97%, showing that the model CRE-MRCNN was able to segment and represent the nodal heads of pork floss more accurately.

3.2. Comparative study

Model evaluation was conducted by comparing this study's proposed

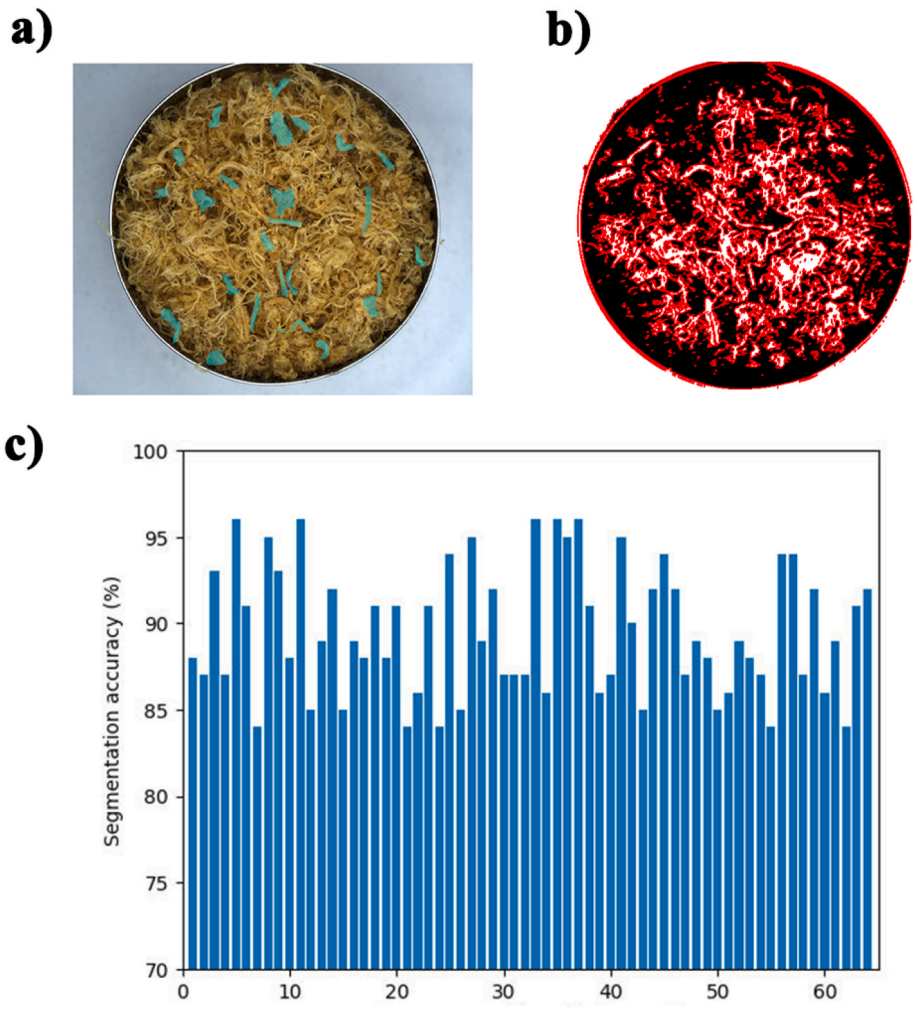

Fig. 5. (a) Pork floss image after labeling knot-head; (b) segmented image according to the already labeled knots; (c) IoU segmentation accuracy graph.

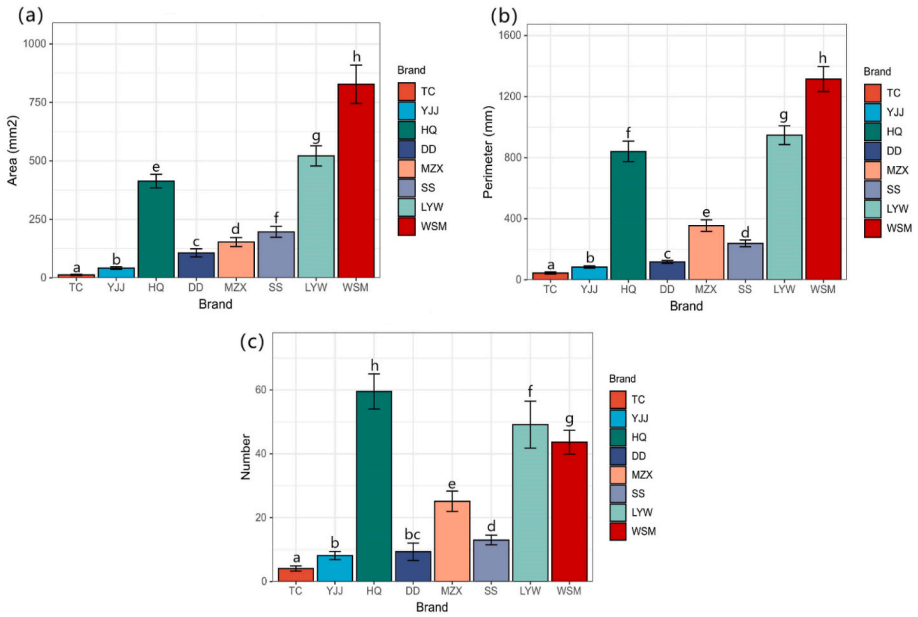

Fig. 6. Information on the characteristics of pork floss knots, (a) total knots area; (b) total circumference of knots; (c) number of knots. Data are expressed as mean ± standard error. Statistical differences between sample groups were shown with different letters (a–h) ($P < 0.05$) according to LSD test.

CRE-MRCNN model with the other methods. The same data were used to experiment with Mask R–CNN, Faster R–CNN, U-net++, Unet 3+, and Cascade Mask R–CNN.

As shown in Table 2, CRE-MRCNN model has the best performance compared to other models on the task of detecting and segmenting the structure feature in pork floss. It can be observed that the CRE-MRCNN model excels in terms of RMSE, accuracy, and ROI compared to the other models. It demonstrates a lower RMSE value, better accuracy, and a larger ROI. These results suggest that the CRE-MRCNN model provides more accurate localization of structure feature in pork floss images, delivering finer segmentation results and thus exhibiting higher reliability and precision in this task.

3.3. Knots feature information

The CRE-MRCNN model for segmenting pork floss images was used to obtain information about the knots of pork floss, including the total area of knots, the total circumference of knots, and the number of knots. In general, the smaller the total area of the knots, the total circumference of the knots and the number of knots, the better the quality characteristics of the pork floss structure.

As can be seen in Fig. 6, the top three pork floss brands in terms of total knot area, total circumference of knot, and number of knots from high to low are WSM, LYW, and HQ, and are significantly above the other pork flosses, including SS, MZX, DD, YJJ, and TC. The ranking of the number of knots from high to low was HQ, WSM, and LYW. It can be seen that WSM, LYW, and HQ had the largest number of knots, indicating that the quality characteristics of these three brands of pork floss was lower. Meanwhile, TC, YJJ, and DD occupied the first three places from bottom to top in terms of total knots area, total circumference of knot, and number of knots. As a result, the proportion of knots in TC, YJJ, and DD is relatively small compared with pork floss of other brands.

3.4. Porosity results

The pore index of pork floss includes porosity, pore number, average pore area, and pore size distribution. By using the CRE-MRCNN model to recognize images of pork floss, the quality characteristics of pork floss structure was evaluated by the pore indices.

As an important indicator to evaluate the microstructure of porous media, porosity is defined as the ratio of void space to total volume of the solid in porous solid media (Rahimi and Ngadi, 2014; Rahimi and Ngadi, 2016). The ratio between the pore area in porous media and the total area of the image region under study is defined as the pore area fraction, and this area is referred to as porosity in 2D planar images (Rovira et al., 2011; Rahimi et al., 2017, 2020). As shown in Fig. 7, the porosities of TC, YJJ, HQ, DD, MZX, SS, LYW, and WSM were 11.74%, 11.98%, 10.45%, 10.61%, 11.12%, 11.65%, 11.96%, and 11.23%, respectively, with no significant differences ($P > 0.05$).

3.5. Pores number results

The coefficient of variation (CV) is an indicator of the degree of dispersion of the variables. The reproducibility of the data is considered good if the CV is <10%, good if 10%–20%, moderate if 20%–30%, and poor if ≥ 30% (Rosner, 2015; Araújo et al., 2020). From Fig. 8a, the mean pore numbers of TC, YJJ, HQ, DD, MZX, SS, LYW, and WSM were 2068, 1491, 1355, 1246, 1179, 1094, 862, and 771, respectively, with significant differences ($P < 0.05$). As shown in Fig. 8b, the within-group CVs (n = 5) for TC, YJJ, HQ, DD, MZX, SS, LYW, and WSM were 4.34%, 2.24%, 3.15%, 3.72%, 3.44%, 7.09%, 4.26%, 3.93%, and the CVs between groups (n = 50) were 6.68%, 4.31%, 4.63%, 5.84%, 4.95%, 8.04%, 6.58%, and 7.70%, respectively. The results showed that the CVs within all groups of pork floss were less than 10%, indicating that the pores number of the eight selected brands of commercially available pork floss were evenly distributed. In addition, the intra-group CV of the pore number of the eight brands of commercially available pork floss was generally lower than the inter-group CV, indicating that the pore number of pork floss in the different groups had some variation in the data, but the variation in the pore number was in a small range.

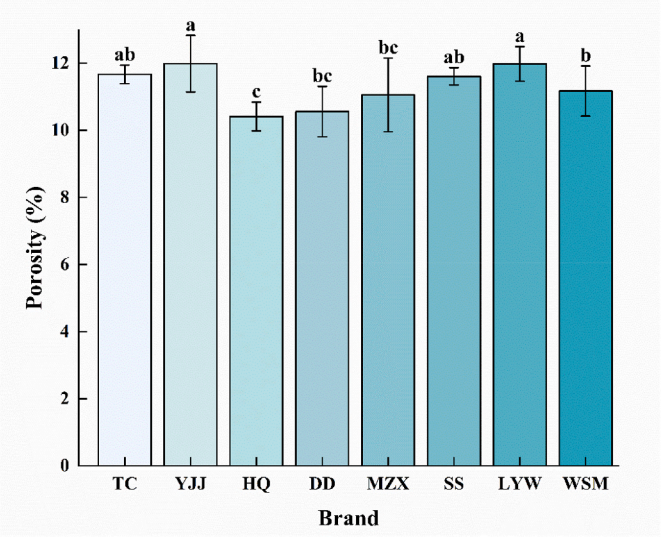

Fig. 7. Porosity of eight commercially available brands of pork floss. Data are expressed as mean ± standard error. Statistical differences between sample groups were shown with different letters (a–c) ($P < 0.05$) according to LSD test.

3.6. Average pore area results

As shown in Fig. 9a, the average pore area of TC, YJJ, HQ, DD, MZX, SS, LYW, and WSM was 0.1127, 0.1246, 0.1458, 0.1852, 0.1860, 0.2358, 0.2416, and 0.2663 mm^2, respectively. From Fig. 9b, it can be seen that the average pore area of pork floss intra-group and inter-group CV was less than 10%. The intra-group CV was generally less than 5%, indicating that the average pore area of the different parts of the same image had low variability and uniform pore size distribution. Inter-group CV values were all below 10%, suggesting that the pore area between multiple groups of images taken with the same brand of pork floss had some differences within a reproducible range.

3.7. Pore size distribution results

Pore size distribution (PSD) is another important property commonly used in microstructural studies of foods. It indicates how frequently pores of different sizes occur in the food structure. Eight brands of pork floss differed in the distribution of the number of pore areas. As can be seen in Fig. 10, the pores are distributed over 0.01–5 mm^2 and there are two distinct peaks in the distribution. The main peak is mainly formed by small pores with pore areas of 0.02, 0.03, 0.04, 0.05, 0.06, 0.07 and 0.08 mm^2 and has the highest value of 0.03 mm^2. It can be seen that the pile of pork floss fibers of each brand has the highest number of pores of 0.03 mm^2. In the distribution of different pore areas, the number of small pores (0.01–0.1 mm^2) distributed in the order TC, YJJ, HQ, DD, MZX, SS, LYW and MZX. There were no significant differences in the distribution of mean pores (0.1–1 mm^2) among the eight brands of pork floss. The second main peak of the distribution was for the large pores with a pore size of 1–5 mm^2. The frequency distribution of the large pore size (1–5 mm^2) was in the order of MZX, LYW, SS, MZX, DD, HQ, YJJ, and TC, in contrast to the order of the small pore size.

3.8. Sensory test results

Due to the peculiarity of the structure of pork floss, the intensity

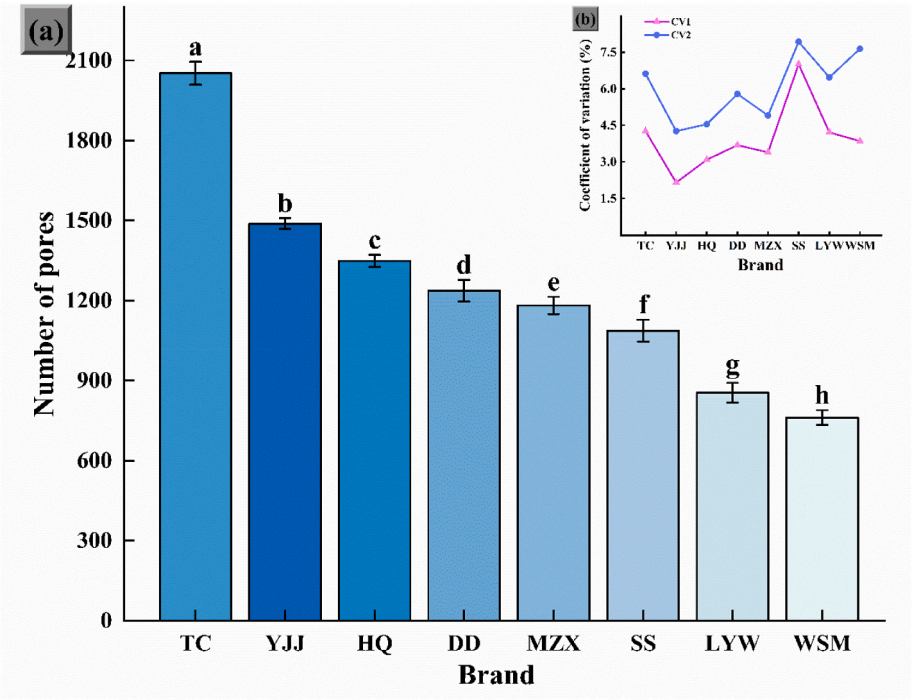

Fig. 8. Pore number of eight brands of pork floss, (a) distribution of pore number of pork floss; (b) coefficient of variation of pore number of eight brands of pork floss, CV1 represents intra-group coefficient of variation, CV2 represents inter-group coefficient of variation. Data are expressed as mean ± standard error. Statistical differences between sample groups were shown with different letters (a–h) ($P < 0.05$) according to LSD test.

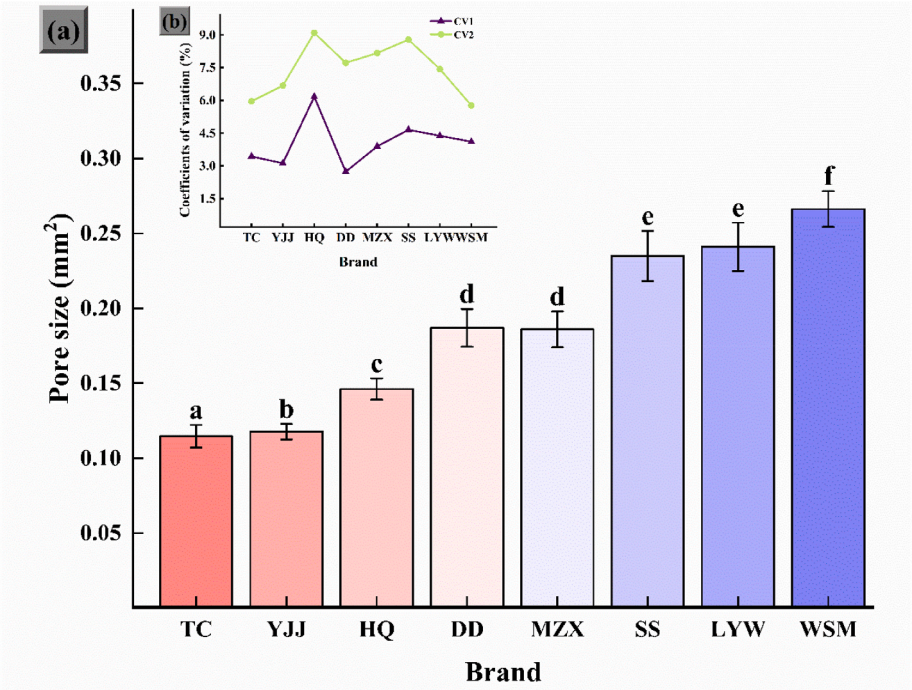

Fig. 9. Average pore area data for eight commercially available brands of meat floss. (a) average pore area of eight brands of meat floss; (b) coefficient of variation of average pore area in eight brands of meat floss, CV1 represents the intra-group coefficient of variation and CV2 represents the inter-group coefficient of variation. Data are expressed as mean ± standard error. Statistical differences between sample groups were shown with different letters (a–f) ($P < 0.05$) according to LSD test.

ratings of each sensory attribute would vary. The lower the intensity of sensory attributes, including knot size, thickness, coarseness, and hardness, the higher the quality characteristics of pork floss. The higher the intensity of sensory attributes, including fluffiness, uniformity, color consistency and intactness, the higher the quality characteristics of pork floss. The results of the sensory test are shown in Table 1. TC had the lowest scores for the attributes knot-head size, coarseness, and hardness attributes (2.95, 3.89, 2.26, respectively) and the second lowest score for thickness (3.25). Similarly, YJJ has the second lowest intensity ratings for the attributes knot size, coarseness, and hardness attributes and the

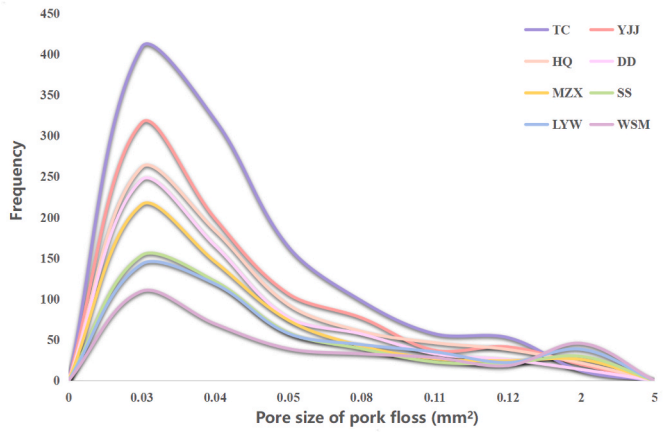

Fig. 10. Pore size distribution of eight commercially available brands of pork floss.

lowest intensity for thickness. While TC had the highest intensity ratings for the attributes of uniformity, color consistency, and intactness (8.24, 8.87, and 7.99, respectively), YJJ had the highest intensity rating for fluffiness (8.47). LYW, WSM, and SS had the highest intensity ratings for knot size, coarseness, hardness, and thickness, and the lowest intensity ratings for fluffiness, uniformity, color consistency, and intactness; intactness was the lowest. Observation indicates that this may be due to the overall unopened fibers of the pork floss with long knots. In terms of liking, TC was the highest, followed by YJJ (7.94), DD (7.43), HQ (6.79), MZX (5.32), SS (4.16), WSM (3.32), and LYW (2.26).

3.9. Comprehensive evaluation model for pork floss

3.9.1. Sensory test-orientated model

The weights of the main indicators were determined by normalizing all data using a gradient descent algorithm. The weights of knot size, thickness, coarseness, hardness, fluffiness, uniformity, color consistency, intactness, and liking were 0.1038, 0.0966, 0.1154, 0.092, 0.1325, 0.1187, 0.1091, 0.1002, and 0.1293, respectively. The positive and negative coefficients of the main factors depended on their effects on the sensory quality of the different brands of pork floss. In this study, higher values for fluffiness, uniformity, color consistency, intactness, and likeability generally had a positive effect on the sensory quality of pork floss, while higher values for knot size, thickness, coarseness, and hardness had a negative effect on the sensory quality of pork floss. Therefore, the overall quality evaluation score of pork floss was calculated as follows:

$$Y = -0.1038 \times \text{knot size} - 0.0966 \times \text{thickness} - 0.1154 \times \text{coarseness} - 0.0924 \times \text{hardness} + 0.1325 \times \text{fluffiness} + 0.1187 \times \text{uniformity} + 0.1091 \times \text{color consistency} + 0.1002 \times \text{integrity} + 0.1293 \times \text{liking}.$$

The corresponding evaluation scores for the different brands of pork floss are shown in Table 3. TC had the highest score (0.9227), followed by YJJ (0.9126), DD (0.8061), HQ (0.7009), SS (0.53875), MZX (0.4437), WSM (0.2902), and LYW (0.2116).

3.9.2. Machine vision-oriented model

For the machine vision-oriented model, the magnitude of the coefficients of the main factors depends on their influence on the quality characteristics of pork floss structure. The weights of total knots area, total circumference of knot, number of knots, porosity, number of pores, average pore area, and pore size distribution were 0.1371, 0.1254, 0.1400, 0.1209, 0.1422, 0.1519, and 0.1818, respectively. The values of porosity, pore number, average pore area, and pore size distribution were within the range of those obtained in this study and generally contributed to a positive effect on the quality characteristics of pork floss structure. In contrast, higher values for total knots area, total circumference of knot, and number of knots tended to have a negative effect on pork floss quality characteristics. Therefore, the overall evaluation of pork floss quality was calculated as follows:

Table 2
Evaluation of each model.

Model	RMSE	ACC	ROI
Cascade Mask R–CNN	0.042	0.935	0.756
Faster R–CNN	0.055	0.902	0.643
Mask R–CNN	0.049	0.918	0.721
U-Net++	0.056	0.896	N/A
UNet 3+	0.048	0.915	N/A
CRE-MRCNN	**0.036**	**0.952**	**0.81**

Table 3
Comprehensive evaluation scores of the computer vision-oriented model and sensory test-oriented model.

Brands	Computer vision-oriented scoring	Sensory test-oriented scoring
TC	**0.816891**	**0.885646146**
YJJ	0.784995	0.789718355
HQ	0.632673	0.653584512
DD	0.646438	0.766037723
MZX	0.606374	0.378186459
SS	0.619669	0.386670692
LYW	0.469013	0.137468943
WSM	0.576314	0.235458244

Table 1
Sensory testing of the fluffy quality in eight commercially available brands of pork floss.

Sensory attributes	Brand							
	TC	YJJ	HQ	DD	MZX	SS	LYW	WSM
Knot-head size	2.95 ± 0.78e	5.04 ± 0.81 d	7.56 ± 0.57c	6.55 ± 0.68 b	7.11 ± 0.81a	8.42 ± 0.54a	7.89 ± 0.88a	8.26 ± 0.77a
Thickness	3.25 ± 0.83 b	1.84 ± 0.69a	7.05 ± 0.74 b	6.49 ± 0.74e	4.26 ± 0.66c	7.84 ± 0.77f	7.68 ± 0.75f	8.16 ± 0.86a
Coarseness	3.89 ± 0.94a	4.69 ± 0.85 b	6.11 ± 0.74 b	5.72 ± 0.88 d	7.74 ± 0.73e	6.16 ± 0.83	4.84 ± 0.69 b	7.11 ± 0.82 d
Hardness	2.26 ± 0.87a	3.79 ± 0.86 b	5.95 ± 0.71c	6.79 ± 1.03 d	7.16 ± 0.83 d	7.89 ± 0.88f	8.21 ± 0.59f	8.16 ± 0.56f
Fluffiness	7.95 ± 0.85f	8.47 ± 0.51f	5.16 ± 0.69e	7.44 ± 0.83 b	2.47 ± 0.70 b	3.84 ± 0.77c	1.63 ± 0.50a	2.32 ± 0.96 b
Uniformity	8.24 ± 0.77f	7.74 ± 0.73f	7.26 ± 0.65 g	6.68 ± 1.00e	4.11 ± 0.94c	4.84 ± 0.57 d	2.89 ± 0.74 b	1.89 ± 0.60a
Color consistency	8.87 ± 0.51c	8.47 ± 0.80c	5.11 ± 0.74 b	6.74 ± 0.87 b	4.68 ± 0.67a	4.05 ± 0.78a	4.42 ± 0.61a	4.21 ± 1.18a
Intactness	7.99 ± 0.86 d	7.84 ± 0.90 d	6.32 ± 0.75 d	6.93 ± 0.73c	5.98 ± 0.91c	6.05 ± 0.91c	4.91 ± 0.78 b	3.79 ± 0.99a
Likeness	8.37 ± 0.60f	7.94 ± 0.94f	6.79 ± 0.79 d	7.43 ± 0.60f	5.32 ± 0.95c	4.16 ± 0.90 b	2.26 ± 0.81a	3.32 ± 1.33 b

Note: Means ± standard errors with different superscripts within a column are significantly different ($P \leq 0.05$) according to Turkey's HSD test (Honestly significant difference).

$$Y = -0.1371 \times \text{total knots area} - 0.1254 \times \text{total circumference of knots} - 0.1400 \times \text{number of knots} + 0.1209 \times \text{pores number} + 0.1422 \times \text{average pore area} + 0.1519 \times \text{porosity} + 0.1818 \times \text{pore size distribution}$$

Table 3 shows the overall evaluation scores of pork floss based on machine vision. TC had the highest score (0.8113), followed by YJJ (0.7797), DD (0.6421), and HQ (0.6284), and the rest were SS (0.6155), MZX (0.6023), WSM (0.5724), and LYW (0.4658).

4. Discussion

The CRE-MRCNN proposed in this study showed better performance. Compared with the results of Hao et al. (2021) and He et al. (2022), the segmentation accuracy of CRE-MRCNN in this study is higher. This is not only the result of the improvement of the Mask R–CNN model, but also may be due to the preprocessing of the images of pork floss. Meanwhile, the parts of the knot and non-knot of pork floss were described manually, which greatly improved the learning ability of the CRE-MRCNN model. The edge contour of the knots in the region of interest was improved by preprocessing, resulting in high segmentation accuracy of the CRE-MRCNN model. CRE-MRCNN also exhibits similarly higher accuracy, lower RMSE, and greater ROI than other deep learning models.

Since pores and knots are important features of the pork floss structure, this requires an evaluation as well as a ranking of the selected commercially available pork floss quality based on the pore and knots features identified by the CRE-MRCNN model. The texture of pork floss may vary due to different production processes. According to Vaskoska et al. (2021), there is an interaction between cooking temperature and lateral shrinkage of fiber fragments. The volumetric shrinkage of fiber fragments increases steadily with increasing temperature. And as cooking time and temperature increase, the number, size, and shape of meat particles are affected (Promeyrat et al., 2010). Therefore, too high processing temperature as well as too long cooking time will lead to more nodules and burnt heads, which will affect the formation of fluffy quality of pork floss. In addition to processing factors, differences in the diameter of pork floss fibers are attributed to the choice of raw materials, including the time of maturation of raw meat after slaughter. In addition, a study by Ao et al. (2015) indicated that the pore number of porous media formed by a large number of fibers is proportional to the fiber diameter. The smaller the fiber diameter, the more pores are formed, the larger the fiber diameter, the smaller the number of pores. It can be seen that the difference in pore diameter is related to the degree of dispersion of the protein fibers of each brand of pork floss. All these factors influence the change of muscle from myofascial to myofibrils and myogenic fibers, resulting in differences in the degree of fiber loosening. The greater the degree of sarcomere fiber opening, the smaller the fiber diameter (with the basic structure of the muscle, the myofibril, being in the range of 10–100 μm) (Sorapukdee et al., 2013). On the contrary, the lower the degree of pork floss fibers opening, the larger the diameter of the pork floss fibers, and the more likely the formation of burnt knots and knots during frying. According to Xia et al. (2020), the quality characteristics of pork floss should not only be velvety and fluffy, but also fine and soft like cotton. Therefore, the size of the fiber diameter not only affects the quality of pork flosses but also the number of pores formed between the fibers. With similar porosity, the smaller the fiber radius, the smaller the average pore radius of porous media formed by the accumulation of many fibers (Zheng et al., 2018). Differences in the number of burnt knots and knots and presentation status affected the pore size when the fibers were stacked (Xia et al., 2020). This is the reason for evaluating different brands of pork floss based on knots and burnt heads and the pore size of pork floss.

TC, YJJ, and DD have better quality and can have fluffy conditions because the proportion of knots is relatively small compared with pork floss of other brands. Meanwhile, the smaller the pore area and the larger the number of pores of pork floss, the better the quality characteristics. TC and YJJ, may present a better fluffiness and are therefore of higher quality. And from the pore sizes distribution, the distribution of pork floss is not uniform, but has a specific aggregation. The pores are unevenly distributed due to the random distribution and arrangement of the fibers during the stacking process (Jha et al., 2020). As the surface density increases, the number of fiber layers on the sample increases accordingly, and some of the large pores are continuously partially covered by the newly added fiber layers, and the number of large pores decreases, so that the pore size is more concentrated in the area with smaller values (Jha et al., 2020). The smaller the pore area and the larger the number of pores of pork floss, the better the quality characteristics. Therefore, the pork floss of TC is more advantageous than other brands of pork floss.

In addition, the machine vision-oriented model provided ranking results for several brands of pork floss that were consistent with the results of the sensory-oriented model. The highest rankings were for the brand TC, followed by YJJ, DD, and HQ. This ranking was consistent with the strength of the sensory test preference. This indicates that the machine vision-oriented model was able to recognize the characteristics of the presented pork floss, including knots and pores. Based on this, the machine vision-oriented model was able to distinguish and identify different brands of pork floss and was able to rank them and select the best pork floss. It is enough to show that the application of machine vision is important to evaluate the quality characteristics of commercially available pork floss structure.

5. Conclusion

In this study, a machine vision-based pork floss feature detection method is proposed, namely CRE-MRCNN, and the model achieves better pork floss image segmentation results. Based on the knot features (total knot area, total circumference of knot, number of knots) and pore features (porosity, number of pores, average pore area and pore size distribution) identified from the pork floss, a comprehensive scoring model was applied to rank the eight brands of pork floss. The highest score was obtained for the TC brand of pork floss, followed by YJJ, DD, and HQ. This result was consistent with the ranking of the sensory test model. The results demonstrate the potential of machine vision techniques for identifying the quality characteristics of pork floss structure. Due to the disordered muscle fibers of pork floss and the varying extent of knots and pores that can occur in different processes. The method provides effective guidance and ideas for identifying different brands of pork floss and solves the problem of difficult identification of pork floss due to its complex and convoluted features. It makes it possible for machine vision technology to be a tool for identification.

CRediT authorship contribution statement

Che Shen: Conceptualization, Investigation, Formal analysis, Data curation, Writing – original draft, Writing – review & editing. **Meiqi Ding:** Data curation, Investigation, Formal analysis. **Xinnan Wu:** Data curation. **Guanhua Cai:** Data curation. **Yun Cai:** Data curation. **Shengmei Gai:** Supervision. **Bo Wang:** Conceptualization, Methodology, Formal analysis, Visualization, Funding acquisition, Writing – review & editing. **Dengyong Liu:** Conceptualization, Project administration, and, Funding acquisition.

Declaration of competing interest

The authors declare that they have no known competing financial interests or personal relationships that could have appeared to influence the work reported in this paper.

Data availability

The data that has been used is confidential.

Acknowledgement

This work was supported by Liaoning Key Laboratory of food safety, Bohai University [LNKLFS202115], Bohai University Postgraduate Innovation Fund Project [YJC2022-014], "the Science and Technology Project of Unveiling and Commanding" from Liaoning Province [2021JH1/10400033], the Open Fund of Institute of Ocean Research, Bohai University [BDHYYJY2023016]. The authors would like to express their gratitude to EditSprings (https://www.editsprings.cn) for the expert linguistic services provided.

References

Ali, H., Tran, S., Garcez, A., Weyde, T., 2014. Convolutional Data: towards Deep Audio Learning from Big Data.

Ao, Q., Wang, J., Tang, H., Zhi, H., Ma, J., Bao, T., 2015. Sound absorption characteristics and structure optimization of porous metal fibrous materials. Rare Met. Mater. Eng. 44 (11), 2646–2650.

Araújo, J., Peçanha, T., Novelli, F., Mello, C., Moreira-Gonçalves, D., Arsa, G., Cambri, L., 2020. Reproducibility of heart rate variability indices at post-maximal exercise. Int. J. Sports Med. 41 (8), 512–519.

Cai, J., Zhu, Y., Ma, R., Thakur, K., Zhang, J., Wei, Z., 2021. Effects of roasting level on physicochemical, sensory, and volatile profiles of soybeans using electronic nose and HS-SPME-GC–MS. Food Chem. 340, 127880 https://doi.org/10.1016/j.foodchem.2020.127880.

Cai, Z., Vasconcelos, N., 2021. Cascade R-CNN: high quality object detection and instance segmentation. IEEE Trans. Pattern Anal. Mach. Intell. 43 (5), 1483–1498. https://doi.org/10.1109/TPAMI.2019.2956516.

Chinese Standards, 2009. Dried Meat Floss (GB/T23968-2009). Retrieved from. http://c.gb688.cn/bzgk/gb/showGb?type=online&hcno=94F4FC8A09A7A5A4EB3B0E3D1B07E7B3.

Esser, S., Löwer, E., Peuker, U., 2021. Network model of porous media – review of old ideas with new methods. Sep. Purif. Technol. 257, 117854 https://doi.org/10.1016/j.seppur.2020.117854.

Fu, J., Thomas, H., Li, C., 2021. Tortuosity of porous media: image analysis and physical simulation. Earth Sci. Rev. 212, 103439 https://doi.org/10.1016/j.earscirev.2020.103439.

Girshick, R., 2015. Fast R-CNN. 2015 IEEE International Conference on Computer Vision (ICCV), Santiago, Chile, pp. 1440–1448. https://doi.org/10.1109/ICCV.2015.169.

Huang, H., Lin, L., Tong, R., Hu, H., Zhang, Q., Iwamoto, Y., Han, X., Chen, Y., Wu, J., 2020. UNet 3+: a full-scale connected UNet for medical image segmentation. vol. 2020. In: ICASSP 2020 - 2020 IEEE International Conference on Acoustics, Speech and Signal Processing (ICASSP), Barcelona, Spain, pp. 1055–1059. https://doi.org/10.1109/ICASSP40776.2020.9053405.

Hao, Z., Lin, L., Post, C.J., Mikhailova, E.A., Li, M., Chen, Y., Yu, K., Liu, J., 2021. Automated tree-crown and height detection in a young forest plantation using mask region-based convolutional neural network (Mask R-CNN). ISPRS J. Photogrammetry Remote Sens. 178, 112–123. https://doi.org/10.1016/j.isprsjprs.2021.06.003.

He, K., Gkioxari, G., Dollar, P., Girshick, R., 2017. Mask R-CNN. International Conference on Computer Vision. IEEE Computer Society.

He, H., Xu, H., Zhang, Y., Gao, K., Li, H., Ma, L., Li, J., 2022. Mask R-CNN based automated identification and extraction of oil well sites. Int. J. Appl. Earth Obs. Geoinf. 112, 102875 https://doi.org/10.1016/j.jag.2022.102875.

Jha, D., Dhekne, P., Patwardhan, A., 2020. Characterization and evaluation of tea bag papers. J. Food Sci. Technol. 57 (8), 3060–3070.

Javadi, S., Dahl, M., Pettersson, M.I., 2020. Adjustable contrast enhancement using fast piecewise linear histogram equalization. In: Proceedings of the 2020 3rd International Conference on Image and Graphics Processing, pp. 57–61.

Lecun, Y., Bengio, Y., Hinton, G., 2015. Deep learning. Nature 521 (7553), 436–444. https://doi.org/10.1038/nature14539.

Li, P., Liu, E., Chen, Z., 2021. Changes in micropore structure and moisture transport properties in fibrous porous media after ultrasound treatment. Heat Mass Transfer 57, 431–439. https://doi.org/10.1007/s00231-020-02962-2.

Li, Y., Wang, G., Nie, L., Wang, Q., Tan, W., 2018. Distance metric optimization driven convolutional neural network for age invariant face recognition. Pattern Recogn. 75, 51–62. https://doi.org/10.1016/j.patcog.2017.10.015.

Münch, B., Holzer, L., 2010. Contradicting geometrical concepts in pore size analysis attained with electron microscopy and mercury intrusion. J. Am. Ceram. Soc. 91 (12), 4059–4067. https://doi.org/10.1111/j.1551-2916.2008.02736.x.

Promeyrat, A., Bax, M., Traoré, S., Aubry, L., Santé-Lhoutellier, V., Gatellier, Ph, 2010. Changed dynamics in myofibrillar protein aggregation as a consequence of heating time and temperature. Meat Sci. 85 (4), 625–631. https://doi.org/10.1016/j.meatsci.2010.03.015.

Rahimi, J., Baur, J., Singh, A., 2020. Digital imaging as a tool to study the structure of porous baked foods. J. Cereal. Sci. 95, 103084 https://doi.org/10.1016/j.jcs.2020.103084.

Rahimi, J., Ngadi, M., 2014. Inter-particle space fractions in fried batter coatings as influenced by batter formulation and pre-drying time. LWT–Food Sci. Technol. 57 (2), 486–493.

Rahimi, J., Ngadi, M., 2016. Structure and irregularities of surface of fried batters studied by fractal dimension and lacunarity analysis. Food Struct. 9, 13–21.

Rahimi, J., Ngadi, M., Agyare, K., Koehler, B., 2017. Oil spots and moisture pocket re-distributions between crust and core regions of potato strips during post-frying holding. Food Struct. 11, 1–7.

Ren, S., He, K., Girshick, R., Sun, J., 2017. Faster R-CNN: towards real-time object detection with region proposal networks. IEEE Trans. Pattern Anal. Mach. Intell. 39 (6), 1137–1149. https://doi.org/10.1109/TPAMI.2016.2577031.

Rosner, B., 2015. Fundamentals of biostatistics. Cengage Learn.

Rovira, S., López, M., Ferrandini, E., Laencina, J., 2011. Hot topic: microstructure quantification by scanning electron microscopy and image analysis of goat cheese curd. J. Dairy Sci. 94 (3), 1091–1097.

Shen, C., Cai, Y., Ding, M., Wu, X., Cai, G., Wang, B., Gai, S., Liu, D., 2023. Predicting VOCs content and roasting methods of lamb shashliks using deep learning combined with chemometrics and sensory evaluation. Food Chem. X 19, 100755. https://doi.org/10.1016/j.fochx.2023.100755.

Shenoy, P., Innings, F., Tammel, K., Fitzpatrick, J., Ahrné, L., 2015. Evaluation of a digital colour imaging system for assessing the mixture quality of spice powder mixes by comparison with a salt conductivity method. Powder Technol. 286, 48–54. https://doi.org/10.1016/j.powtec.2015.07.034.

Song, Z., Zhang, J., Xun, X., Liu, B., Bu, X., 2021. A Mask-RCNN based quantification method for pigmentation of cephalopod beaks. Fish. Moderniz. 48 (5), 70–78 (in Chinese).

Sorapukdee, S., Kongtasorn, C., Benjakul, S., Visessanguan, W., 2013. Influences of muscle composition and structure of pork from different breeds on stability and textural properties of cooked meat emulsion. Food Chem. 138 (2–3), 1892–1901. https://doi.org/10.1016/j.foodchem.2012.10.121.

Taheri-Garavand, A., Fatahi, S., Omid, M., Makino, Y., 2019a. Meat quality evaluation based on computer vision technique: a review - sciencedirect. Meat Sci. 156, 183–195. https://doi.org/10.1016/j.meatsci.2019.06.002.

Taheri-Garavand, A., Fatahi, S., Shahbazi, F., de la Guardia, M., 2019b. A nondestructive intelligent approach to real-time evaluation of chicken meat freshness based on computer vision technique. J. Food Process. Eng. 42, e13039.

Vaskoska, R., Ha, M., Ong, L., Chen, G., White, J., Gras, S., Warner, R., 2021. Myosin sensitivity to thermal denaturation explains differences in water loss and shrinkage during cooking in muscles of distinct fibre types. Meat Sci. 179, 108521 https://doi.org/10.1016/j.meatsci.2021.108521.

Wang, B., Shen, C., Cai, Y., Dai, L., Gai, S., Liu, D., 2023. Consumer culture in traditional food market: the influence of Chinese consumers to the cultural construction of Chinese barbecue. Food Control 143, 109311. https://doi.org/10.1016/j.foodcont.2022.109311.

Xia, W., Gai, S., Liu, D., 2020. Effect of postmortem aging time on quality characteristics of dried meat floss. Meat research 34 (6), 85–90.

Zhang, J., Meng, Y., Wu, J., Qin, J., Yu, S., 2020. Monitoring sugar crystallization with deep neural networks. J. Food Eng. 280, 109965 https://doi.org/10.1016/j.jfoodeng.2020.109965.

Zheng, Q., Fan, J., Xu, C., 2018. Fractal model of gas diffusion through porous fibrous materials with rough surfaces. Fractals 26, 1850065 (05).

Zhou, Z., Rahman Siddiquee, M.M., Tajbakhsh, N., Liang, J., 2018. UNet++: a nested U-net architecture for medical image segmentation. In: Stoyanov, D., et al. (Eds.), Deep Learning in Medical Image Analysis and Multimodal Learning for Clinical Decision Support. DLMIA ML-CDS 2018 2018, Lecture Notes in Computer Science, vol. 11045. Springer, Cham. https://doi.org/10.1007/978-3-030-00889-5_1.